**WEST-EAST HIGH SPEED FLOW FIELD CONFERENCE**
**19-22, November 2007**
**Moscow, Russia**

# VALIDATION OF AERODYNAMIC DESIGN TECHNOLOGY OF SUPERSONIC EXPERIMENTAL AIRPLANE (NEXST-1) BY FLIGHT TEST

**Dong-Youn Kwak* Naoko Tokugawa** and Kenji Yoshida***

** Aviation Program Group, Japan Aerospace Exploration Agency*
*6-13-1, Osawa, Mitaka, Tokyo, 181-0015, Japan*
*Email: kwak.dongyoun@jaxa.jp, yoshida.kenji@jaxa.jp, web page:http://www.jaxa.jp*
*** Institute of Aerospace Technology, Japan Aerospace Exploration Agency*
*7-44-1 Jindaiji-Higashimachi, Chofu, Tokyo, 182-8522, Japan*
*Email:tokugawa.naoko@jaxa.jp*

**Key words:** SST, Flight test, Aerodynamic design, Drag reduction, CFD

**Abstract.** Flight test of a supersonic experimental airplane was performed by Japan Aerospace Exploration Agency to improve advanced aerodynamic design technologies for the next generation SST. The experimental airplane was designed to reduce the drag on a supersonic cruise condition. Surface pressure distributions, boundary layer transition locations and aerodynamic forces in the flight test were obtained to demonstrate the aerodynamic design methods and tools. The flight test results evaluated by comparing with the prediction results obtained by CFD based optimum design tools. The flight test results relatively corresponded to the CFD results. Aerodynamic design concepts for drag reduction were demonstrated qualitatively and quantitatively by the NEXST-1 flight test.

## 1. INTRODUCTION

A research for the next generation SST named NEXST (National Experimental Supersonic Transport) program had been advanced by JAXA (Japan Aerospace Exploration Agency)[1,2]. The NEXST program consists of fundamental research activities of the future SST technologies and a supersonic experimental airplane (NEXST-1) project. The NEXST-1 project is concentrated on developing an unmanned and non-powered supersonic experimental airplane to demonstrate supersonic aerodynamic design technology, and to accumulate unmanned flight technology. The drag reduction on the supersonic cruise condition is set to a goal on aerodynamic design of the NEXST-1. The conventional and advanced concepts to reduce the drag are applied to the

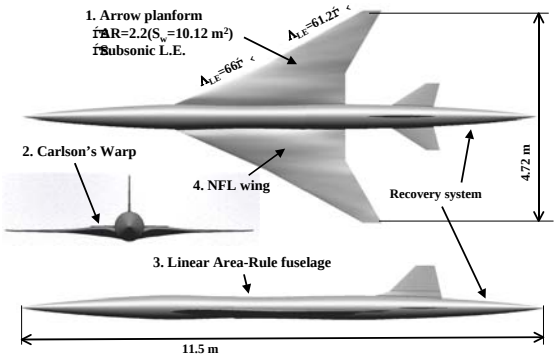


Fig.1 Schematics of the NEXST-1 configuration

aerodynamic design[3,4]. An optimized geometry of the NEXST-1 could be designed by using a CFD-based inverse method. The NEXST-1 was also designed as a small scaled airplane with the size of 11 percents of an actual scale SST (Fig.1). Supersonic flight test was planned to demonstrate and verify the aerodynamic design technologies. The flight test was successfully conducted on Oct. 10. 2005 at Woomera test range in Australia[5,6]. In the flight test, three types of aerodynamic data were measured to validate the design methods and tools. Validation of the aerodynamic design technology on the NEXST-1 by the flight test introduce in this paper.

## 2. AERODYNAMIC DESIGNS

### 2.1. Design concepts

The Aerodynamic design of the NEXST-1 was conducted to reduce the drag on the supersonic cruise condition of Mach 2.0 and the lift coefficient $C_L$=0.1. The following four design concepts were applied to the NEXST-1[4]; 1) arrow planform wing, 2) warped wing, 3) area-ruled fuselage and 4) natural laminar flow wing (Fig.1).

*Arrow planform wing* : From the supersonic linear theory[7], a wing with higher aspect ratio and highly swept leading edge is desirable planform at supersonic speed. An arrow planform wing with an optimum slenderness ratio is selected in compromising aerodynamics and structural constraints.

*Warped wing* : To reduce the lift-dependent drag, a warped wing design was conducted by using the Carlson's method[8]. The optimum load distribution can be obtained by the optimum combination of the wing camber and twist distributions that called "warped surface". The key point of the warp design is to suppress the theoretical infinite load at leading edge. It means that attached flow is achieved by leading edge droop.

*Area-ruled body* : According to the supersonic slender body theory[9], the wave drag due to volume of a complete aircraft is generally related to the supersonic cross sectional area distribution. If a wing and tails of a complete aircraft are specified, we suppose that fuselage geometry should be improved to adjust supersonic area distributions of the equivalent axisymmetrical body to that of Sears-Haack body. Those area-ruled body design is very useful for reducing the interference drag among the between wing, tails and fuselage.

*Natural Laminar Flow wing* : A laminar airfoil design concept is usually based on suppressing Tollmien-Schlichting (T-S) wave instability. For a low aspect ratio wing with highly swept leading edge, transition due to cross-flow (C-F) instability is dominant at forward part of the wing. Therefore, to suppress both the T-S and the C-F instabilities, we found an optimum pressure distribution that had sharply increased pressure gradient at the narrow region of the front part of the wing, and had gradual pressure gradient at other chord locations. This pressure distribution was derived using a practical transition prediction method based on $e^n$ method[4,10,11] and selected as a target pressure distribution on the upper surface in our NLF (Natural Laminar Flow) wing design.

### 2.2. Design tools

The wing geometry was obtained by JAXA's CFD-based inverse design method[12]. CFD analysis for the aerodynamic design of the NEXST-1 was conducted using UPACS

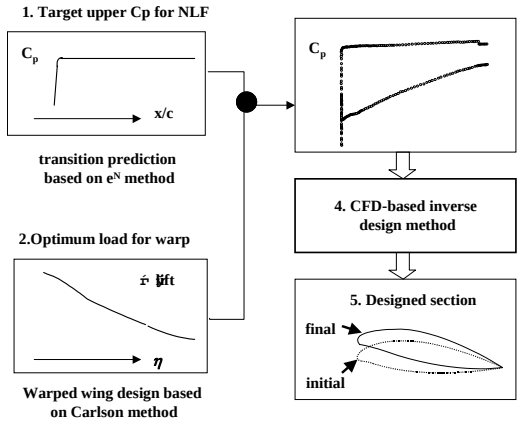


Fig.2 Aerodynamic design process by using the CFD-based inverse method

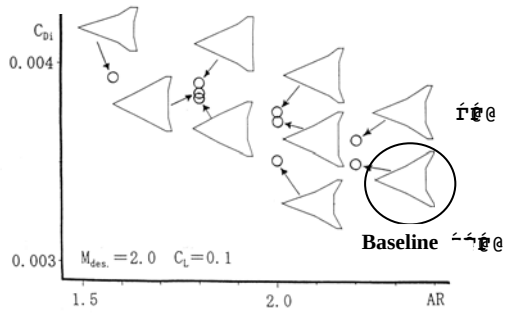


Fig.3 Aerodynamic design of the wing planform

(Unified Platform for Aerospace Computation Simulation) code that was developed in JAXA. Details to the CFD analysis were reported in reference 13. Governing equation of the UPACS was Navier-Stoked code using S-A turbulence model. Figure 2 shows the procedure of the CFD-based inversed design method. NLF wing design tools derived the target surface pressure $C_p$ distributions on the upper surface. And lower surface optimum $C_p$ distributions were derived from the optimum load distributions along the spanwise direction by the warped wing design tools. The optimum wing section geometries were derived through the iterating modification of the wing sections to make its $C_p$ distributions according with the optimum $C_p$ distributions.

### 2.3. Design process

The aerodynamic design process using the design concepts or principles above consisted of two stages. At the first stage, a baseline configuration was designed using a supersonic linear theory, namely lifting surface and slender body theory. At first, eight wing planforms were selected from the parametric study of the wing planforms evaluating the drag-polar characteristics. Then, a baseline wing planform was selected from eight wing planforms by conducting the warped wing design (Fig.3). Also, area ruled fuselage design was conducted to reduce the wave drag referred the Sears-Haack body. At the second stage, some refinements of the baseline were performed by CFD (N-S codes) analysis, to improve the limitation based on the linear theory. Then to improve the lift-to-drag ratio, an optimum configuration was designed applying the natural laminar flow wing concepts. The optimum warped wing design was conducted again with fixed upper surface geometry of the wing and the area ruled fuselage. Detail of the design process was reported in reference 4.

## 3. WIND TUNNEL TEST

Wind tunnel tests were conducted to validate the CFD-based design tools and the aerodynamic design concepts on the wind tunnel test conditions. The wind tunnel tests were performed at 1m×1m supersonic wind tunnel in JAXA. A small scaled NEXST-1 model with 8.5 percents scaled were used to the wind tunnel tests.

Figure 4 shows the $C_p$ distributions at the design point. Although, small different from the CFD results and the wind tunnel test results were observed near the leading edge, overall $C_p$ distributions on both results show good agreement. The agreement of the $C_p$

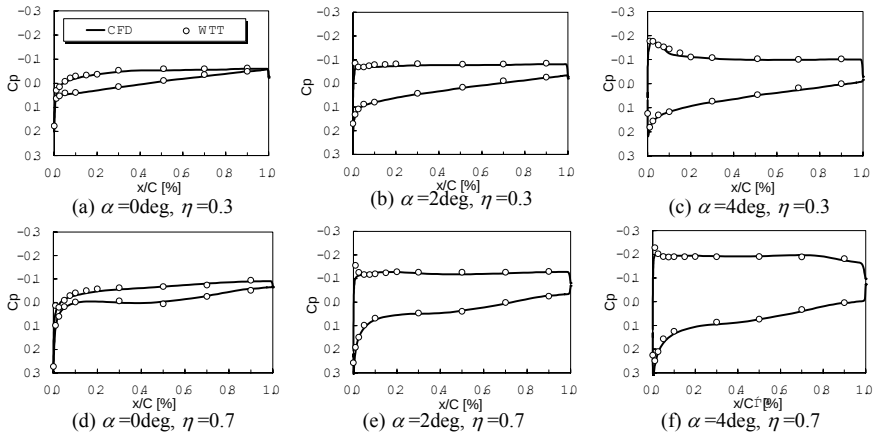


Fig.4 $C_p$ distributions from CFD analysis and wind tunnel test (M=2.0)

distributions on both results means the optimum $C_p$ distributions were also achieved from the wind tunnel tests[13]. It means that the aerodynamic design tools were verified from the wind tunnel tests. The locations of the boundary layer transition measured from the wind tunnel tests[14]. The boundary layer transition locations were more delayed at the design point than those at off-design points. Similar trend was observed from other wind tunnel test at S2MA in ONERA (Office National d'Etudes et Recherches Aérospatiales) [15] with 23 percent scaled NEXST-1 model. The delay of the transition at the design point and the agreement of the $C_p$ distributions at the upper surface were cleared that the NLF wing design concept was validated from the wind tunnel test.

In this section, the verification of the CFD based design tools and the validations of the aerodynamic design concepts were confirmed from the wind tunnel tests. However, Reynolds number on the wind tunnel test conditions is lower than that on the flight condition of the actual scale SST. And the freestream turbulence level on the wind tunnel tests is larger than that on the flight test. The aerodynamic data at high Reynolds number and at without freestream turbulence can be obtained from the NEXST-1 flight test.

## 4. FLIGHT TEST

### 4.1. Overall of the flight test

Figure 5 shows the overall flight test plan[6]. A solid rocket brings the NEXST-1 to the appropriate conditions (Mach number and the altitude, etc.), and then the NEXST-1 separates from the rocket, and starts to glide by the auto-pilot system. There are two aerodynamic measurement phases near the altitude $H$=18km and 12km at $M$=2.0. The first measurement phase is called "$\alpha$-sweep", the other phase is called "*Re*-sweep". At the $\alpha$-sweep measurement phase, the angle of attack changes to six steps by pitch-and-pause. The fourth step of the $\alpha$-sweep is a design point ($M$=2.0, $C_L$=0.1, $H$=18km). Hence, aerodynamic data can be obtained on the design point and off-design points at same Mach number and Reynolds number flight conditions. At the *Re*-sweep measurement phase, the aerodynamic data at $M$=2.0 and $C_L$=0.1 can be obtained on the conditions of high Reynolds number comparing with data at the $\alpha$-sweep phase. After these measurement phases, the NEXST-1 decelerates by consuming the energy, and then touches down softly to the ground by the parachutes and airbags.

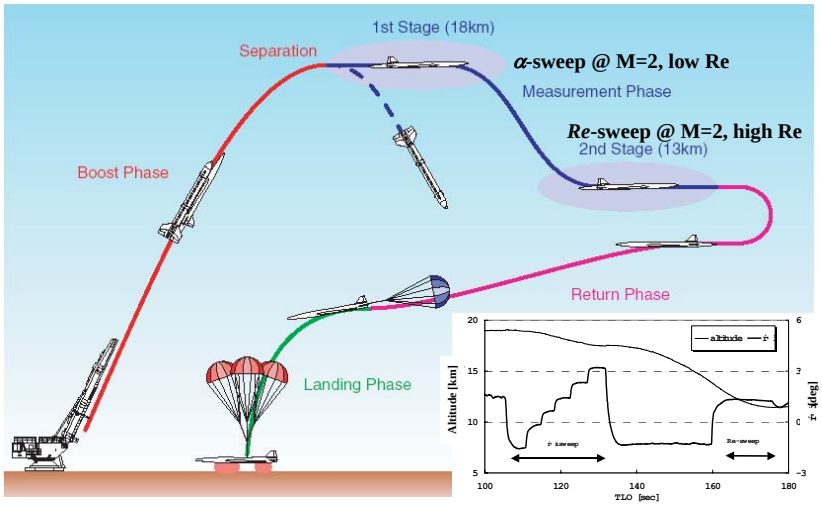


Fig.5 Overall flight test plan

The flight test of the NEXST-1 was conducted on October. 10. 2005 at Woomera test range, Australia[5]. The flight test was completely performed in all sequences as scheduled, and the NEXST-1 was recovered safely. A number of aerodynamic data could be acquired from the flight test. Figure 6 shows the flight trajectory during the aerodynamic measurement phases. During the measurement phases, the Mach number kept a constant value at $M$=2.0 with small tolerance of $\Delta M$=±0.05. Six values of $\alpha$ were obtained with pitch-and-pause that corresponded to the $\alpha$-sweep as scheduled. The Reynolds number has slightly changed during the $\alpha$-sweep phase that is obvious different the Reynolds number at the *Re*-sweep phase. Flight test data for evaluate aerodynamic design concepts were selected the data at each steps on which the data settled down to a constant value that plotted on Fig.6(a).

## 4.2. Aerodynamic measurement systems

To verify the aerodynamic design concepts, three types of aerodynamic data were measured; 1) Surface pressure distributions, 2) Boundary layer transition locations and 3) Aerodynamic forces. Aerodynamic measurement systems were designed to measure aerodynamic data with high accuracy and reliability in the flight test. Figure 7 shows locations of aerodynamic sensor installed on the NEXST-1. A part of the sensors for transition location detection are located on the port side of the airplane, and surface pressure tappings are installed on the other side. A Pitot tube (ADS probe) is mounted on the starboard side of the nose (Fig.8) to measure the flight conditions ($M$, $\alpha$, $\beta$, etc.). Reference 14,16-19 reported in details to the measurement systems for the flight tests.

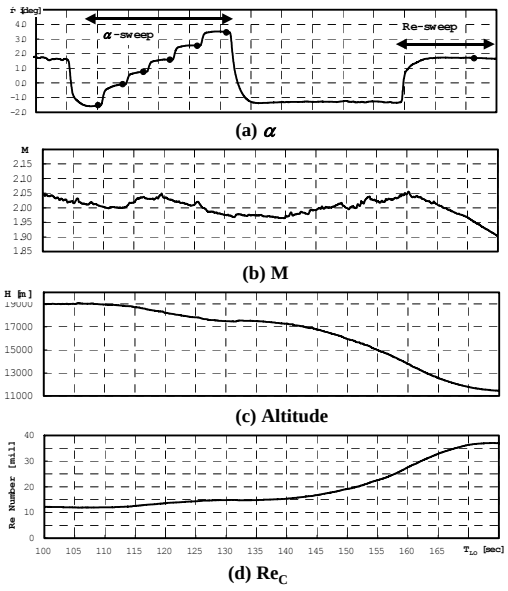


Fig.6 Flight trajectory at the aerodynamic measurement phases

Surface static pressures were measured at the 313 points of the pressure tappings (Fig.7). Seven differential type pressure

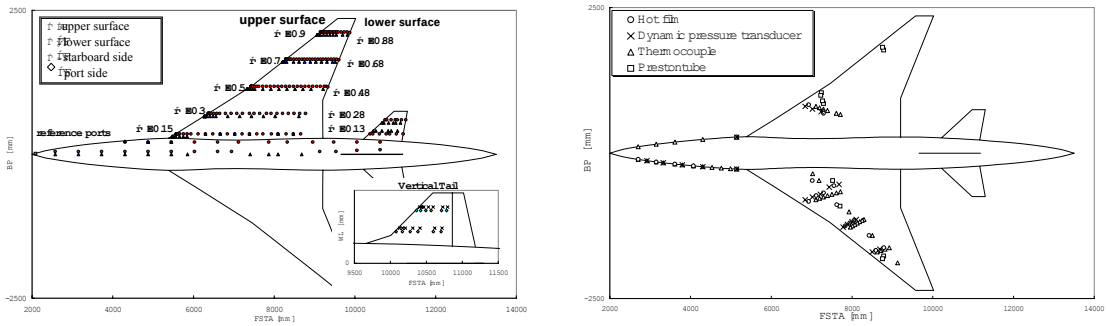


(a) Locations of the static surface pressure

(b) Locations of the transition measurement sensors

Fig.7 Locations of the aerodynamic measurement sensors

scanners (ZOC 33; Scanivalve Corp.) are equipped on the fuselage for surface pressure measurement (Fig.8). A pressure tapping for the reference pressure is installed near the nose. The reference pressure is connected to each pressure scanners (for the back pressure) and an absolute type pressure transducer (CAT-130-1; TKK). The estimated overall uncertainty of the pressure coefficient $C_P$ is less than ±0.0115 at 100:1 odds[16].

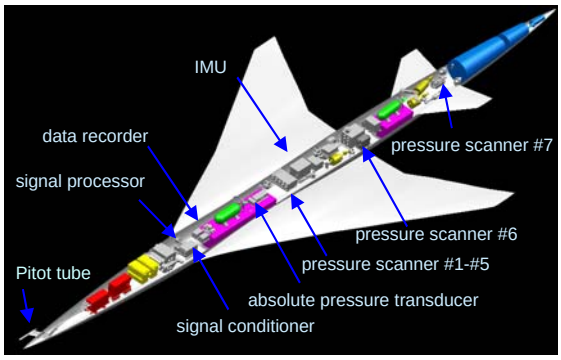


Fig.8 Layout of the instruments for the aerodynamic measurement

Four types of sensors, which are used to detect the transition location in the NEXST-1, are hot-film sensor (HF), dynamic pressure transducer (DP), thermocouple (TMP), and Preston tube (Pr). These sensors are installed on the NEXST-1 surface with an inclination of 15~20° on the wing side to the flow direction. Therefore, the upstream sensor does not disturb the downstream boundary layer (Fig.7). Details of the measurement systems for the boundary layer transition locations were referred to reference 14,17,18. The transition measurement systems were checked by the wind tunnel test in which the sensors and systems for the transition measurements were actually same to those on the NEXST-1. The correlations of the results by four types of sensors were also confirmed.

Six components aerodynamic forces and moments are measured by using an inertial measurement unit (IMU: H-764J/G Honeywell)[19]. To improve the accuracy of the aerodynamic forces on the flight test, some corrections were conducted.

### 4.3. Flight test results

In this chapter, aerodynamic data obtained from the flight test will evaluate using the CFD analysis results [13,17,20,21]. Effects by the static aeroelastic deformation and the boundary layer transition locations were considered on the CFD analysis to coincide the flight test conditions. Details of the static aeroelastic deformation and the transition locations were reported in reference 13,22.

The NEXST-1 was manufactured to a production shape that deformed to the optimum designed shape at the design point of the flight test. However, deformed shapes at the off-design points are different from the optimum designed shape. Therefore, static aeroelastic analysis consisted of FEM and CFD analysis was conducted to the main wing of the NEXST-1[22] at each steps ($\alpha$-sweep and $Re$-sweep phases). The forebody deformation was suggested by results of a structural static loading tests. Thus, the angle

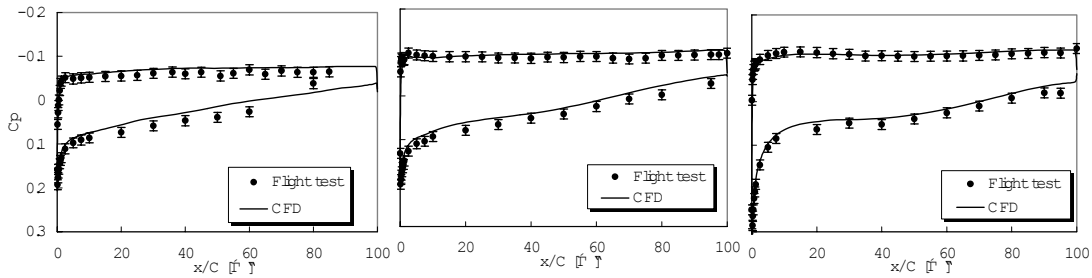


(a) $\eta$=0.3 (b) $\eta$=0.5 (c) $\eta$=0.7

Fig.9 $C_p$ distributions at the design point at the several spanwise locations at the $\alpha$-sweep phase (M=2.0, $\alpha$=1.59deg)

of attack measured by the Pitot tube must be corrected, because the Pitot tube is installed near the nose of the forebody (Fig.8). As a mentioned above, the NEXST-1 was designed to the NLF wing. Then the CFD analysis considered the boundary layer transition locations were conducted to evaluate the benefits of the NLF wing design. Information of the boundary layer transition locations of the wing were obtained from the flight test results measured by the transition measurement sensors. The laminar flow CFD analysis was conducted at the area that upstream of the transition lines, while the turbulent flow CFD analysis was performed to the area that downstream of the transition lines[13]. From the consideration of the above two effects, the conditions of the CFD analysis can coincide to the flight test conditions.

### *Surface pressure distributions*

Figure 9 shows pressure coefficient $C_P$ distributions at the design point at the several spanwsie locations obtained by the flight test. The error-bars on the $C_P$ distributions are the uncertainty of the pressure measurement system mentioned above section. $C_P$ distributions by the CFD analysis are also plotted in Fig.9. $C_P$ distributions by the flight test relatively correspond to the CFD results. Abrupt changes of the pressure are observed near the leading edge, and gradual pressure gradient are observed at the rear part of the local chord length.

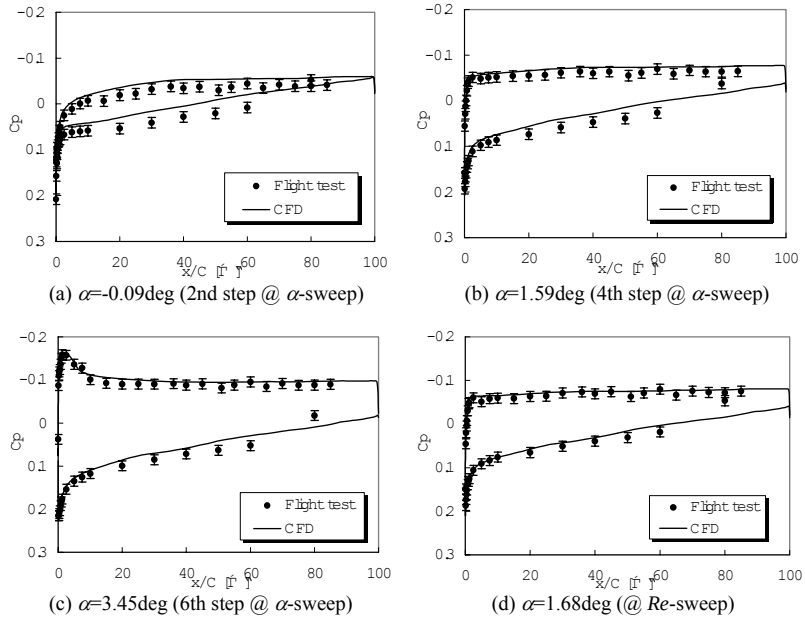


(a) $\alpha$=-0.09deg (2nd step @ $\alpha$-sweep) (b) $\alpha$=1.59deg (4th step @ $\alpha$-sweep)

(c) $\alpha$=3.45deg (6th step @ $\alpha$-sweep) (d) $\alpha$=1.68deg (@ *Re*-sweep)

Fig.10 $C_p$ distributions at the $\alpha$-sweep phase and the *Re*-sweep phase (M=2.0, $\eta$=0.3)

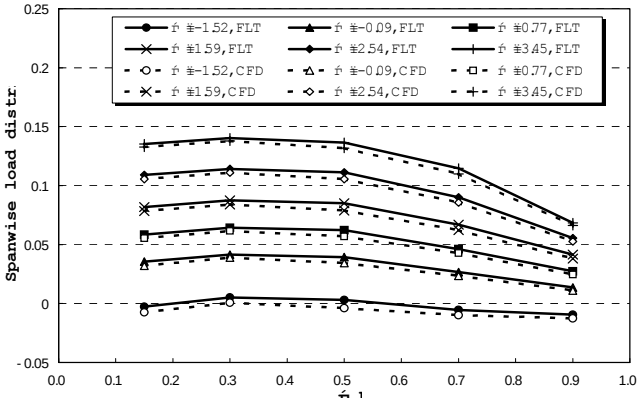


Fig.11 Spanwise load distributions at the $\alpha$–sweep phase

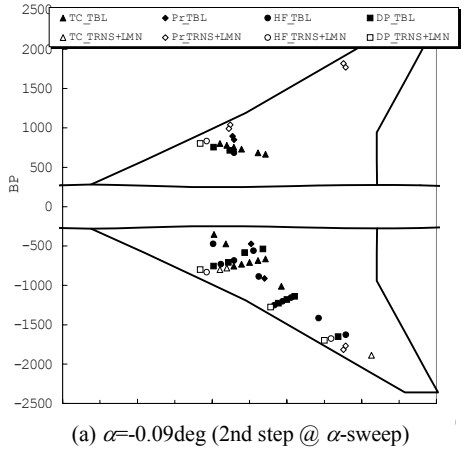


(a) $\alpha$=-0.09deg (2nd step @ $\alpha$-sweep)

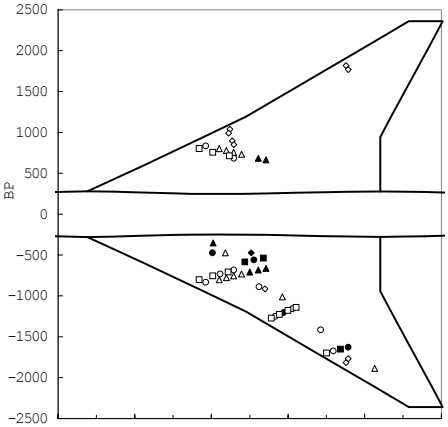


(b) $\alpha$=1.59deg (4th step @ $\alpha$-sweep)

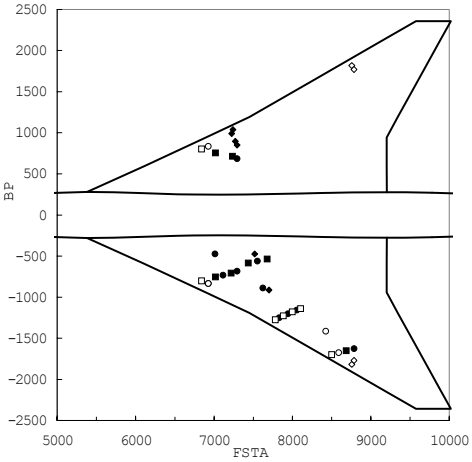


(c) $\alpha$=1.68deg @ *Re*-sweep

Fig.12 Transition location distributions at the aerodynamic measurement phases (M=2.0)

However, the $C_P$ distributions on the upper surface at 6th step of the $\alpha$-sweep ($\alpha$=3.45deg) indicate that adverse pressure gradient observed near the leading edge (Fig.10). It means that the $C_P$ distributions at $\alpha$=3.45deg deviate from the $C_P$ distribution of the NLF wing. The $C_P$ distributions on the lower surface at $\eta$=0.3, $\alpha$=-0.09deg (2nd step) are different at both results. It was suggested that those differences were related to the geometry of the inner wing or fuselage. Further analysis should be performed to understand the discrepancies of the $C_P$ distributions in the flight test and the CFD results. Figure 11 shows spanwise load distributions at several angles of attack. The load distributions are obtained from integrating measured $C_P$ distributions. The CFD results are also obtained through same process of the flight test. The pressure coefficient distributions in the flight test relatively correspond to the CFD results that are target distributions obtained by the optimum design.

### *Boundary layer transition locations*

The transition location of the boundary layer on the wing upper surface can directly validate the NLF wing design concept. Detail data processing and the data analysis of the transition measurements are described on reference 14,17,18.

The flow conditions of the boundary layer were defined using the analysis of the four kinds of sensors according to objective criteria[17,18]. Figure 12 shows the transition location distributions at the 2nd and 4th steps of the $\alpha$-sweep phase, and the *Re*-sweep phase. The NEXST-1 wing geometry is plotted to the figure. The symbols (circle, triangle, rectangular and diamond symbols) on the figure correspond to the locations of

each sensor. The flow condition of the boundary layer was classified into two conditions; the laminar or transitional states and the turbulent states. The open symbols mean the laminar and transitional boundary layers, and solid symbols mean the turbulent boundary layers. The boundary layer transition from the transitional states to the turbulent states will be occurred at a location between the open symbols and the solid symbols. The data from a part of the thermocouple that can not determine the flow condition were not plotted to the Fig.12. Relatively good correlations were observed on the transition measurement results by the four types of the sensors. It is cleared that the transition location at the 4th step of the $\alpha$-sweep phase moves further downstream than the location at the 2nd step. The upper surface $C_P$ distributions at the 4th step was achieved the optimum $C_P$ distributions for the NLF wing (see Fig.9). Therefore, these favorable $C_P$ distributions suppressed the cross-flow instability and the T-S type instability. Comparing with the transition locations at different Reynolds number based on a mean aerodynamic chord length ($Re_C$) but a same $\alpha$, the transition locations at the 4th step of the $\alpha$-sweep ($Re_C$ =14.0×10$^6$) were delayed than that at the *Re*-sweep phase ($Re_C$=34.7×10$^6$). These results mean the optimum $C_P$ distribution on the upper surface for the NLF wing is very sensitive to the Reynolds number. From this result, propriety of the NLF wing design at the design point ($C_L$=0.1 at $M$=2.0 and $H$=18 km) is confirmed.

The NLF wing concept was confirmed from the flight test at high Reynolds number and no freestream disturbance conditions. Numerical prediction of the boundary layer transition was also performed using the LSTAB[23] developed by JAXA. These flight test results of the boundary layer transition are very valuable data to improve the accuracy of the numerical prediction technique.

### *Aerodynamic forces*

Figure 13 shows $C_L$-$\alpha$ results on the flight test (symbols). CFD results also plotted on the figure (curves). The gradient of the $C_L$ curve obtained by the CFD corresponds to the flight test results. Whereas, the value of the $C_L$ measured by the flight test on the $\alpha$-sweep phase are slightly larger than the CFD results. The load distribution (Fig.11) on the flight test and the CFD results were also observed similar tendency. However, good agreement of the flight test results on the *Re*-sweep with the CFD results were observed. We are conducting further analysis and inspection to understand the discrepancy that observed on the flight test results with the CFD results.

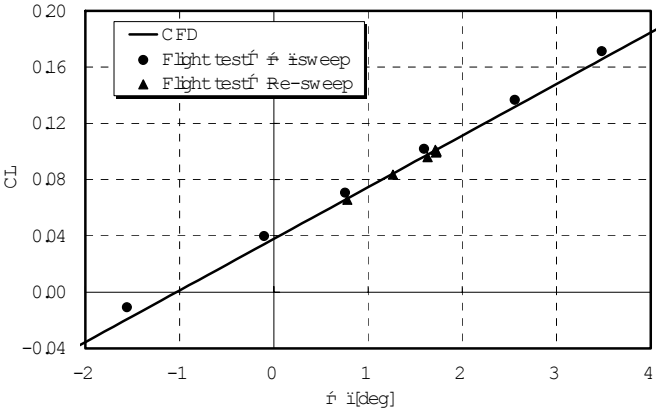


Fig.13 $C_L$-$\alpha$ characteristics at the aerodynamic measurement phase (M=2.0)

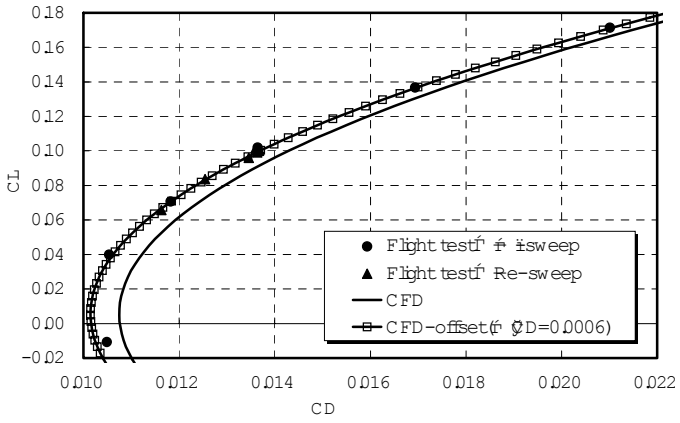


Fig.14 The drag polar characteristics at the $\alpha$-sweep phase

Figure 14 shows the drag polar characteristics. Comparing with both results, the minimum value of the drag $C_{D\,min}$ on the flight test is different from the CFD results. When the drag polar curve obtained by the CFD shifts 6 counts (=0.0006) to the left along the horizontal axis (rectangular symbols with solid line on Fig.14), the CFD result corresponds to the flight result well. It means that though minimum drag on the flight result is different with the CFD results, the profile of the drag polar curve corresponds with each other. In general, the profile of the drag polar depends on the wing planform, and a lift at the minimum drag $C_{L0}$ depends on the warp design. Therefore, good agreements of the drag polar profile and $C_{L0}$ in both results mean that the aerodynamic design tools of the wing planform and warped wing can validate by the flight test.

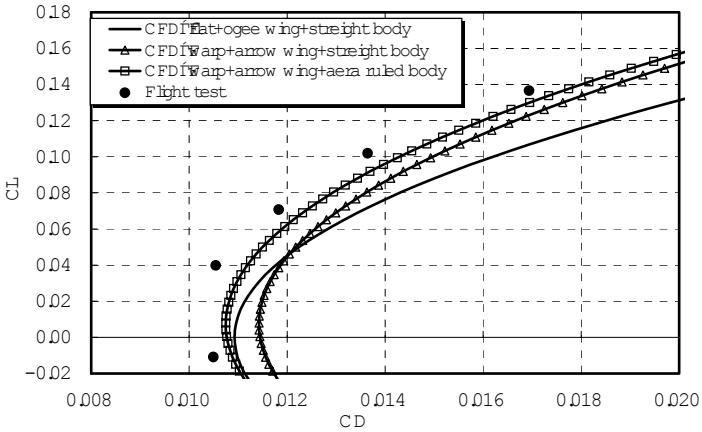


Fig.15 The benefits of the each aerodynamic design concepts at the $\alpha$-sweep phase

Figure 15 shows the drag polar characteristics by CFD analysis to clear the benefits of each aerodynamic design concepts; the arrow wing planform, the area ruled fuselage and the warped wing. The solid line on Fig.15 corresponds to the results of flat ogee wing with the straight body. This configuration is not applied above three design concepts. The triangle symbols correspond to the results of the warped arrow wing planform also with the straight body. Comparing with the solid line and the triangle symbols, the benefits of the arrow wing planform and the warped wing will be cleared. Furthermore, the rectangular symbols correspond to the results of the warped arrow wing planform with the area ruled body. Comparing with those three curves, each benefit of the aerodynamic design concepts was cleared. The benefits of the each concept are larger than the accuracy of the flight test results. This means that the benefits of the each design concepts could be resolved from the flight test.

## 5. AERODYNAMIC DESIGN FOR REAL SCALE SST

From above chapter, we confirmed the validity of the aerodynamic design of the NEXST-1 from the supersonic flight test. At the next step, we designed an actual scale SST by means of the same aerodynamic design concepts and methods as the NEXST-1. The four aerodynamic design concepts for the drag reduction mentioned above were also applied to the actual scale SST.

The size of the SST decided to 91m lengths that assumed 300 passengers. The design point is also same as the cruise condition of the NEXST-1. Therefore, the Reynolds number at the cruise conditions of the SST is much higher than that of the NEXST-1. However, the transition locations at the *Re*-sweep phase were not delayed comparing with transition locations at the 4th steps of the $\alpha$-sweep phase (Fig.12). It means that the benefit of the NLF wing observed at the $\alpha$-sweep phase of the NEXST-1 flight test is not achieved at higher Reynolds number. Therefore, the improved NLF wing design tools can find another optimum $C_P$ distributions that have the robustness on the variation of the *Re*. The wing geometry at high Reynolds number was derived from the

optimum $C_P$ distributions. When the value of the $N$ in the $e^N$ method selects 12.5 from the flight test results, the transition locations on the upper wing surface could be delayed to the 45 percent of the local chord length. Figure 16 shows the configuration of the real scale SST that obtained by the inverse design methods same as the NEXST-1. Details of the aerodynamic design of the real scale SST were evaluated in reference 13. We confirmed from the recent study that the real scale SST could improve the aerodynamic performance compared with a conventional SST geometry[13]. In this section, it was shown that the aerodynamic design tools and methods that established from the NEXST-1 could be applied to the aerodynamic design of the actual scale SST.

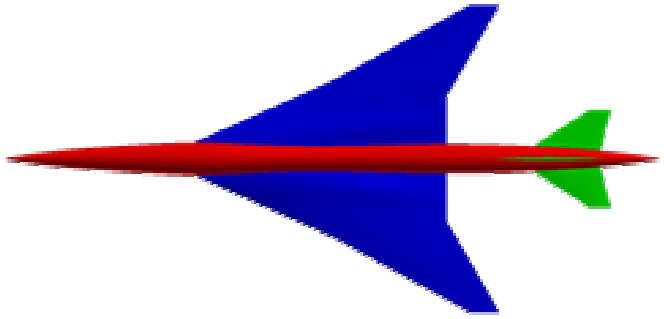

Fig.16 Configuration of the actual scale SST

## 6. CONCLUSION

Flight test of a supersonic experimental airplane was conducted to validate advanced aerodynamic design tools and methods. The experimental airplane is designed to reduce the drag at supersonic cruise condition. The flight test results evaluated by comparing with prediction results obtained from the CFD based optimum design tools. Pressure coefficient distributions from the flight test relatively corresponded to the CFD results that are target distributions. The boundary layer transition locations on the wing measured from the flight test were more delayed at the design point than those at the off-design points. The profile of the drag polar curve on the flight test also corresponded to the CFD results. Aerodynamic design concepts for the drag reduction were demonstrated qualitatively and quantitatively by the NEXST-1 flight test.

Further analysis of the flight test will be performed to understand the reason of any discrepancy with the CFD analysis and to improve the accuracy of the CFD analysis and the flight test results.

## 7. ACKNOWLEDGMENTS

The authors gratefully acknowledge to the staff of Mitsubishi Heavy Industries, Ltd., Kawasaki Heavy Industries, Ltd. and Fuji Heavy Industries, Ltd. for their contribution of the flight test of the NEXST-1. The authors greatly thank to Mr. H. Ishikawa, Mr. M. Noguchi for their helpful support on the CFD analysis and the wind tunnel tests.

## 8. REFERENCES

[1] K. Sakata, “Supersonic Experimental Airplane (NEXST) for Next Generation SST Technology - Development and Flight Test Plane for the Unmanned Scaled Supersonic Glider- ”, AIAA Paper 2002-0527 (2002).

[2] T. Ohnuki, K. Hirako and K. Sakata, "National Experimental Supersonic Transport Project", *International Congress of the Aeronautical Science,* 2006-1.4.1 (2006).

[3] K. Yoshida, "Overview of NAL's Program Including the Aerodynamic Design of the Scaled Supersonic Airplane", held at the VKI, RTO Educational Notes 4, 15.1-16 (1998).

[4] K. Yoshida and Y. Makino,"Aerodynamic Design of Unmanned and Scaled Supersonic Experimental Airplane in Japan", ECCOMAS 2004, Finland, Jul. (2004).

[5] P. Nikoloff and T. Onuki, "Woomera Test Range and the Launch of the NEXST-1 Supersonic Flight Trial Experiment", Aerospace Testing Expo 2005, North America, Nov. (2005).

[6] T. Fujiwara, K. Hirako and T. Ohnuki,"Flight Plan and Flight Test Results of Experimental SST Vehicle NEXST-1", *International Congress of the Aeronautical Science,* 2006-6.2.1 (2006).

[7] F.R.S. Kuchemann, "*The Aerodynamic Design of Aircraft"*, Pergamon Press (1978).

[8] H. W. Carlson and D. S. Miller, "Numerical Method for the Design and Analysis of Wings at Supersonic Speed", NASA TN D-7713 (1974).

[9] H. Ashley and M. Landahl, "*Aerodynamics of Wings and Bodies"*, Dover Publications Inc. (1965).

[10] H. Ogoshi, "Aerodynamic Design of a Supersonic Airplane Wing – Application of the Natural Laminar Flow Concept to Airfoil", Proceedings of the 47th National Congress of Theoretical & Applied Mechanics, Jan. (1998) (in Japanese).

[11] D. Arnal, "Boundary Layer Transition Predictions Based on Linear Theory", AGARD Report No.793 (1993).

[12] S. Jeong, K. Matsushima, T. Iwamiya, S. Obayashi and K. Nakahashi, "Inverse Design Method for Wings of Supersonic Transport", AIAA Paper 98-0602 (1998).

[13] H. Ishikawa, D.Y. Kwak and K. Yoshida, "CFD Analysis on Flight Test Results of Supersonic Experimental Airplane NEXST-1", AIAA Paper 2007-3925 (2007).

[14] D.Y. Kwak, K. Yoshida, M. Noguchi and H. Ishikwa, "Boundary Layer Transition Measurement using Preston tube on NEXST-1 Flight Test", AIAA Paper 2007-4173 (2007).

[15] H. Sugiura, K. Yoshida, N. Tokugawa, S. Takagi and A. Nishizawa, "Transition Measurement on the Natural Laminar Flow Wing at Mach 2", *Journal of Aircraft*, Vol.39, No.6, 996-1002 (2002).

[16] D.Y. Kwak, K. Yoshida, H. Ishikwa and M. Noguchi, "Flight Test Measurements of Surface Pressure on Unmanned Scaled Supersonic Experimental Airplane", AIAA Paper 2006-3483 (2006).

[17] N. Tokugawa and K. Yoshida, "Transition Detection on Supersonic Natural Laminar Flow Wing in the Flight", AIAA Paper 2006-3165 (2006).

[18] N. Tokugawa, D.Y. Kwak and K. Yoshida, "Transition Measurement System of Experimental Supersonic Transport "NEXST-1", *International Congress of the Aeronautical Science,* 2006-3.3.2 (2006).

[19] K. Yoshida, D.Y. Kwak, N. Tokugawa and Y. Makino,"Supersonic Experimental Airplane (NEXST-1) -Aerodynamics and Measurement System Design –", 37th Japan Society for Aeronautical and Space Science Annual Conference, Mar. (2006) (in Japanese).

[20] D.Y. Kwak, N. Tokugawa and K. Yoshida,"Demonstration of Aerodynamic Design Technologies on Supersonic Experimental Airplane (NEXST-1) by Flight Test", Proceedings of 2006 KSAS-JSASS Joint International Symposium on Aerospace Engineering, 176-182 (2006).

[21] K. Yoshida, "Flight Test Results of Supersonic Experimental Airplane (NEXST-1)", *Japanese Journal NAGARE*, Vol. 25, No.4, 321-328 (2006) (in Japanese).

[22] H. Kawakami, T. Takatoya and H. Ishikawa, "Static Aeroelastic Analysis of Supersonic Experimental Airplane NEXST-1 Flight Test", AIAA Paper 2007-4174 (2007).

[23] Y. Ueda, H. Ishikawa and K. Yoshida, "Three Dimensional Boundary Layer Transition Analysis in Supersonic Flow Using a Navier-Stokes Code", *International Congress of the Aeronautical Science,* 2004-2.8.2 (2004).